

Amplitude modulated near-wall cycle in a turbulent boundary layer under an adverse pressure gradient*

A. DRÓŹDŹ, W. ELSNER

*Institute of Thermal Machinery
Częstochowa University of Technology
Al. Armii Krajowej 21
42-201 Częstochowa, Poland
e-mails: arturdr@imc.pcz.czyst.pl, welsner@imc.pcz.czyst.pl*

THIS PAPER PRESENTS the effect of amplitude modulation of small-scale turbulence by large-scale structures in a turbulent boundary layer subjected to an adverse pressure gradient. The results have been compared with the literature data for high Reynolds number, zero-pressure gradient cases (MATHIS *et al.* [1]). It was observed that for relatively low-Reynolds-number turbulent boundary layer ($Re_\tau \approx 1000$) subjected to the adverse pressure gradient, apart from the inner peak of streamwise velocity fluctuations u , a second maximum located in the outer zone of turbulent boundary layer appears. It was found that the large-scale motions are much more energetic for adverse pressure gradients compared with the zero gradient case and the pressure gradient affects mostly the outer region of the flow. Using the method proposed by MATHIS *et al.* [1], based on the correlation function and Hilbert transform, we obtained a clear evidence of a strong correlation between small inner-layer and large log-layer structures, which is similar to that observed for high Reynolds number zero-pressure gradient cases. A simple model of modulation process occurring in adverse pressure gradient boundary layer has been proposed.

Key words: near wall cycle, inner-outer flow interaction, adverse pressure gradient.

Copyright © 2013 by IPPT PAN

Notations

- β Clauser pressure parameter,
- d probe wire diameter,
- δ boundary layer thickness,
- E_W wavelet energy,
- Φ_{uu} probability density function of velocity component spectrum,
- $H\{x(t)\}$ Hilbert transform of $x(t)$ signal,
- k_x streamwise wave number,
- l length of probe wire,
- L large scale component,
- λ_x streamwise length scale,
- p_∞ static pressure of the free-stream,
- R correlation coefficient,

*The paper was presented at XX KKMP conference, Gliwice, 17–20 September, 2012.

Re_θ	Reynolds number based on momentum thickness,
Re_τ	Reynolds number based on friction velocity,
ρ	flow density,
S	small scale component,
S_g	dimensionless distance from inlet plane $S_g = x_s/L$,
t	time,
Tu	turbulence intensity of the free stream $Tu = u/U_0$,
τ_w	wall shear stress,
τ	time scale,
θ	momentum thickness,
U	mean velocity components in streamwise direction,
u_τ	friction velocity,
u^+	dimensionless velocity $u^+ = U/u_\tau$,
u	fluctuating velocity components in streamwise direction,
u'	rms values of fluctuating velocity components in streamwise direction,
ν	kinematic viscosity,
x, y ,	streamwise, wall-normal and spanwise coordinates,
x_s	longitudinal distance from inlet plane,
y^+	dimensionless distance from the wall in inner scaling,
$+$	inner scale symbol,
$\langle \rangle$	conditional averaging.

Abbreviations:

rms	root mean square,
APG	adverse pressure gradient,
ZPG	zero pressure gradient,
TBL	turbulent boundary layer.

1. Introduction

IT IS WIDELY ACCEPTED that significant part of wall turbulence consists of coherent vortical motion or coherent structures. THEODORSEN [2] proposed a model of a hairpin vortex, as a simple flow structure that explains the existence of the low-speed streamwise streaks inducing the ejection event of the near-wall fluid into a higher part of the boundary layer. This hairpin vortex consists of two counter-rotating vortices (legs) connected with the head inclined at approximately 45° to the wall as it is shown in Fig. 1a. According to STANISLAS *et al.* [3], such a symmetrical hairpin rarely exists and the flow is dominated instead by asymmetrical hairpins. ADRIAN *et al.* [4] proposed the concept of a hairpin packet (Fig. 1b), according to which a number of hairpins are aligned in a train in the streamwise direction. In that model long low speed streaks are induced by the heads as well as by the legs of hairpin vortices. Outside the legs the high speed flow regions called sweeps are present. Such long low- and high-speed streaks have been observed by HUTCHINS and MARUSIC [5] who call them “superstructure” events due to their large size and because they account for majority of Reynolds shear stress across the logarithmic layer (GANA-

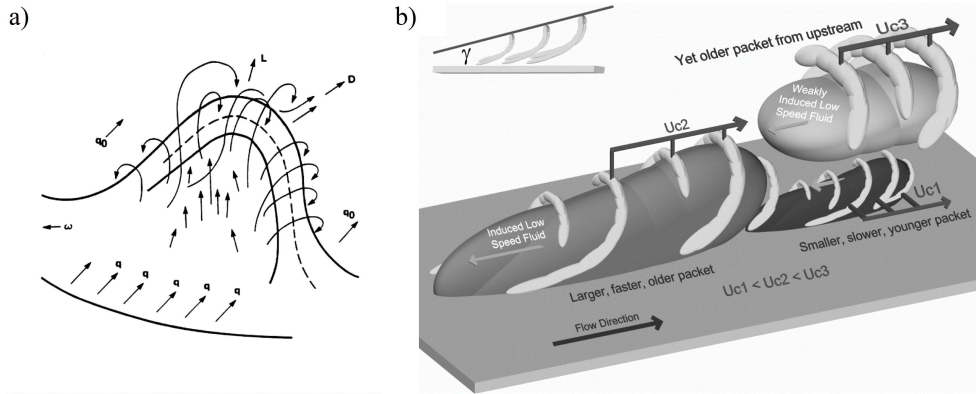


FIG. 1. Theodorsen's hairpin vortex [2]: a) the arrows on either side of the hairpin indicate the direction of the flow, b) very large scale-motion model of ADRIAN *et al.* [4] in which hairpin packets align to produce the long, low-momentum streaks.

PATHISUBRAMAN *et al.* [6]). Recently MATHIS *et al.* [1] have found the existence of coupling between the large-scale component of the velocity signal (referring to the “superstructure” events) and amplitudes of the small-scale signal component in the near-wall region (referring to “near-wall turbulence production cycle”) of high-Reynolds-number ZPG TBLs. Their conclusions were formulated based on analysis performed on an experimental data set extracted from turbulent boundary layer at wide range of Reynolds number. The authors showed that, once the pre-multiplied energy spectrum $k_x \Phi_{uu}/u_\tau^2$ of streamwise velocity component is analysed, the two distinct peaks exist (Fig. 2). Figure 2 shows that the inner and

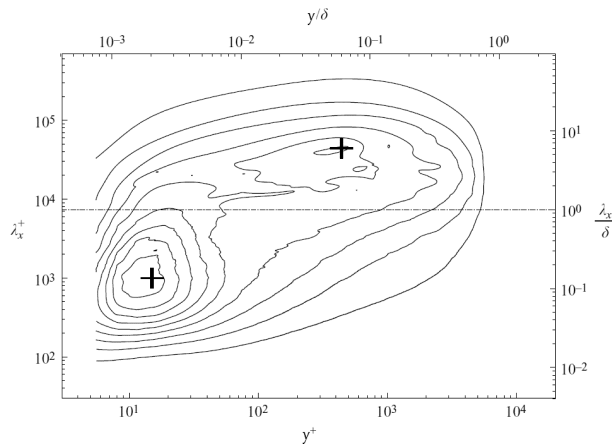


FIG. 2. Iso-contours of the pre-multiplied energy spectra of streamwise velocity fluctuation $k_x \Phi_{uu}/u_\tau^2$. Contour levels are formed from 0.2 to 2.0 in steps of 0.2. The horizontal dotted-dashed lines show the location of the spectral filters [1].

outer peaks, marked by +, are clearly separated in wave number space. The first peak located close to the wall is a footprint of energy originated from low and high speed streaks scaled on viscous units (KLINE *et al.* [7]). The location of this peak is invariable in viscous length scale: $y^+ = 15$ and $\lambda_x^+ = 1000$. The second distinct peak referred to as the outer peak, which according to [1] originates from the superstructure type events observed in the log layer. As opposed to the inner peak the location of the outer peak scales on the outer scale, i.e., boundary layer thickness and its location are found to be the center of the logarithmic layer. Further study of [1] shows that the outer peak on the pre-multiplied energy spectra increases with the Reynolds number, and that the coupling process between scales is stronger in the buffer layer. Recently, HARUN *et al.* [8] demonstrated the strengthening of the modulation process in the buffer layer for the moderate pressure gradient.

It was also proved [1] that the appearance of that outer peak has a direct connection with the existence of the coupling process present in the buffer layer for $\text{Re}_\tau = u_\tau \delta / \nu \gtrsim 1700$, where $u_\tau = \sqrt{\tau_w / \rho}$ is a friction velocity. It also coincidences with energy increase in the log region. That phenomenon was not observed for lower Reynolds numbers, because of insufficient separation of the inner and outer peak scales.

It leads to conclusions that large-scale components play an important role at high Reynolds number wall bounded flows and could have important implications in the active control of turbulence such as reduction of drag or increase of lift force.

From a practical point of view, more important is the knowledge about the coupling between scales in the turbulent boundary layer under the impact of pressure gradient and especially adverse pressure gradient (APG). Motivation for the present paper was built upon the investigations of the mean flow under APG conditions performed by MATERNY *et al.* [9], and analysis of bursting structures behavior in APG region by DRÓZDŹ *et al.* [10] and DRÓZDŹ and ELSNER [11]. The aim of the present work is to study the coupling process between large-scale log region motions and the near-wall turbulence production cycle in adverse pressure gradient turbulent boundary layer at Reynolds number lower than was investigated by MATHIS *et al.* [1] and HARUN *et al.* [8].

2. Experimental setup

To investigate the effect of the coupling between large- and small-scales in the TBL under APG conditions an experimental study has been undertaken. Measurements of the velocity field using the single-wire probe were performed in an open-circuit wind tunnel, where the TBL developed along the flat plate which was 2807 mm long and 250 mm wide. The upper wall of the test sec-

tion was shaped according to the assumed distribution of the pressure gradient corresponding to the conditions encountered in axial compressor blading (Fig. 3b). The velocity at the inlet plane outside the boundary layer was 15 m/s, while the turbulence intensity equaled $Tu = 0.4\%$. Tripping of boundary layer, after the flat plate leading edge, allowed us to obtain a value of Reynolds number $Re_\tau \approx 1000$. For the purpose of the current investigations two cross-sections were selected. The first one located in near zero pressure gradient region ($Sg = 0.185$) marked as ZPG and the second one located in the adverse pressure gradient region ($Sg = 0.597$) marked as APG, where the pressure parameter $\beta = (\delta^*/\tau_w) (dP_\infty/dx)$ is equal to 4.1. The cross-sections in the region of APG flow are located slightly downstream of the maximum of APG (see Fig. 3b). The locations of the cross-sections are shown in Fig. 3 by black dashed lines. The velocity measurements were done with the modified single-wire probe (Dantec Dynamics 55P31) of a diameter $d = 3 \mu\text{m}$ and length in viscous units $l^+ < 20$. The single-wire probe was combined with the DISA 55M hot-wire anemometer connected to 14-bit PC card. Acquisition was maintained at frequency 50 kHz with 10 seconds sampling records.

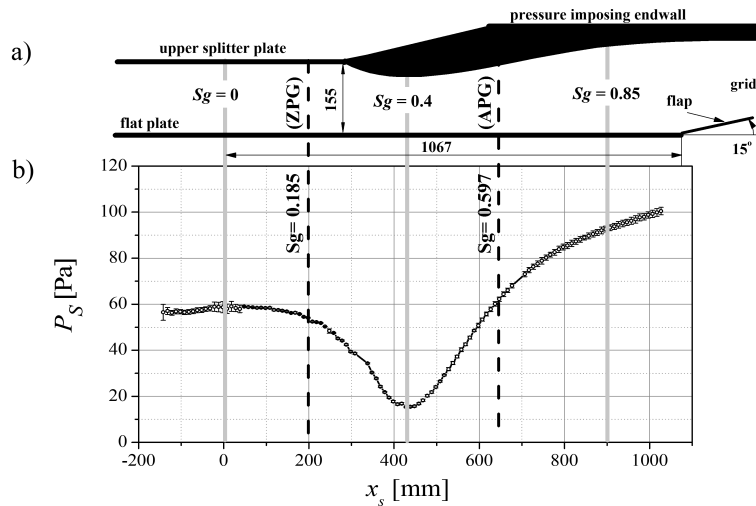


FIG. 3. a) The view of test section; b) corresponding static pressure distribution along the plate.

3. Flow characteristics

Studies presented in [9] showed that for the low-Reynolds-number flow, $Re_\tau \approx 1000$, under APG conditions the similar outer peak as for high-Reynolds-number ZPG TBL is noticed. Its presence suggests a strong coupling between large- and small-scales. Analysis of the mean flow quantities of the TBL under

APG performed in [9] shows that the near-wall region grows much more slowly than the outer part of the boundary layer, which in turn implies that most contributions to boundary layer growth originate from the region located far from the wall. It was confirmed by the appearance of the outer peak of fluctuations, located in the range of $y^+ = 100 \div 300$, which drives the downstream development of TBL.

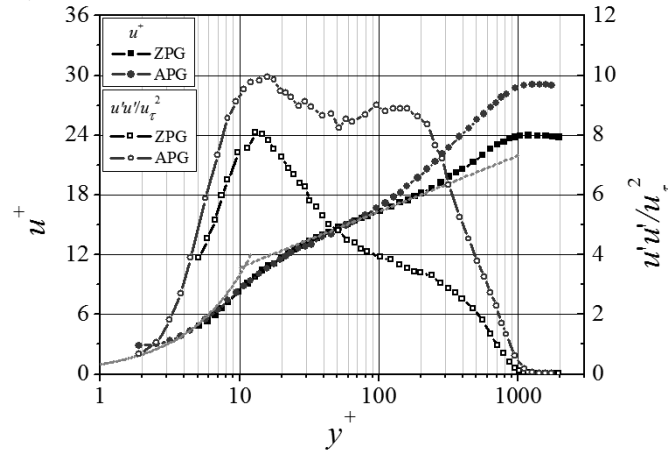


FIG. 4. Velocity profiles and normal $u'u'$ Reynolds stresses in the viscous units at ZPG and APG regions of CUT experiment; u' – fluctuating streamwise velocity.

Figure 4 presents the mean velocity profile u^+ and Reynolds stresses of the $u'u'$ for two chosen cross-sections from ZPG (grey) and APG (dark) conditions. One can observe the significant difference between these two cases. The profile of the mean velocity in the APG region is different from the ZPG flows. In particular, the difference is observed in the wake region as a positive shift of u^+ . For APG flows, apart from the well-known inner peak of $u'u'$ located at $y^+ \approx 15$, the apparent outer peak is observed at the location $y^+ \approx 120$. The magnitude of this peak is almost the same as the inner one and in non-dimensional viscous units it constantly increases downstream of the flow, which is not shown, however, in the graph. It indicates the possibility of the appearance of the outer peak in the energy spectrum. Therefore, the first task was to analyse and compare the energy spectra in the wider range of scales for ZPG and APG flows. In order to estimate the energy distribution for the defined range of scales, the energy spectrum using wavelet transformation was calculated for all measured points across the boundary layer thickness. To obtain the wavelet transform of each recorded signal the Mexican hat wavelet function was used. According to GORDEYEV [12] such a wavelet function is the best choice to perform the analysis of the single events in the time signal.

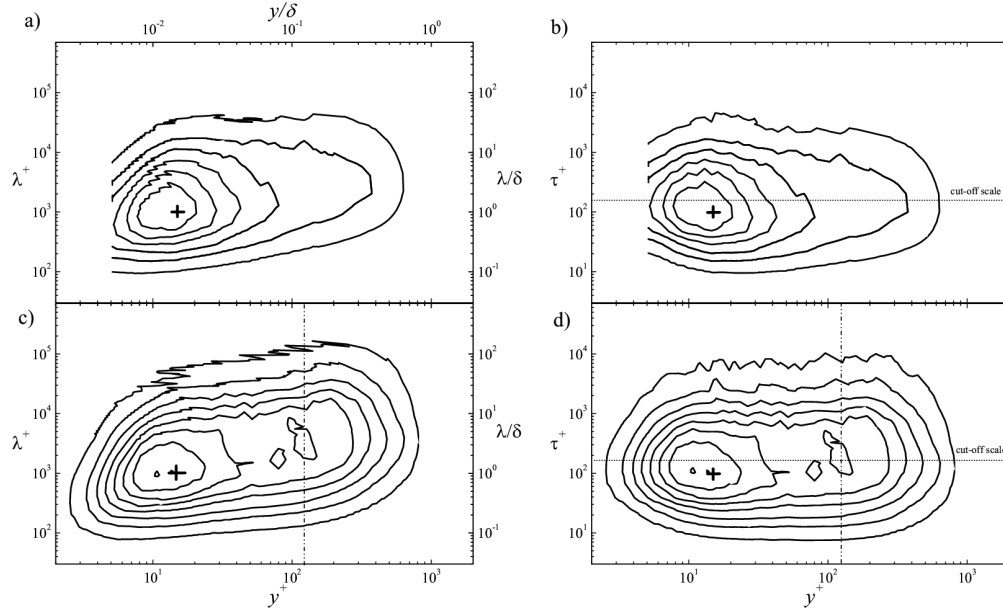


FIG. 5. Iso-contours of the wavelet energy spectra E_W/u_τ^2 across boundary layer thickness for ZPG and APG conditions ($Sg = 0.185$, $Sg = 0.597$) in function of: a) length scale (ZPG), b) time scale (ZPG), c) length scale (APG), d) time scale (APG). Contour levels are from 0.3 to 2.4 in steps of 0.3. The horizontal dotted lines show the location of the spectral filter, while vertical dotted-dashed lines show the location of the outer peak in the APG flow ($y/\delta = 0.12$, $\lambda_x/\delta \approx 3$).

Iso-contours of the wavelet energy spectra E_W , scaled by the friction velocity, as a function of the y^+ are presented in Fig. 5. The left set of figures (Figs. 5a and 5c) presents spectra as a function of the length scale λ^+ , while the right set of figures (Figs. 5b and 5d) as a function of the time scale τ^+ , both in viscous units. In order to switch between these two kinds of scales the mean local velocity was used. The first peak (+), corresponding to the small-scale component, is clearly visible for both cases and its intensity is of similar amplitude indicating that small scales remain almost unaffected by pressure gradient. On the other hand, the substantial rise of energy is observed for APG for a larger scales $\lambda_x > \delta$. The outer peak occurs at location $y/\delta \approx 0.12$ for $\lambda_x \approx 3\delta$, which is only slightly different from the position shown in [8]. One should note, however, that the outer peak position (see [1]) is Reynolds number dependent. It can be assumed that it is a similar phenomenon to that observed by MATHIS *et al.* [1] for the ZPG, and MONTY *et al.* [13] as well as HARUN *et al.* [8] for the moderate APG flows. To confirm the assumptions it was decided to perform analysis aimed to detect interaction between large log-layer and small inner-layer scales.

4. Methodology

In order to study the coupling process the method proposed in [5] was used. This method utilises the correlation function of the single velocity signal, which has to be specially processed. The velocity signal is decomposed into small and large-scale components using high- and low-pass filtering. During the first step the filtered small-scale component has to be specially prepared in order to obtain the envelope of the signal amplitude. In order to extract not only the information about the amplitude, but also about the derivative of the signal the small-scale component u_S has to be additionally processed by the Hilbert transform:

$$(4.1) \quad H\{u_S\} = \frac{1}{\pi} \int_{-\infty}^{+\infty} \frac{u_S(\tau)}{t - \tau} dt.$$

One important property of the Hilbert transform is

$$(4.2) \quad H\{\cos(t)\} = \sin(t), \quad H\{\sin(t)\} = -\cos(t).$$

The envelope of the amplitude of the signal and its derivative can be calculated by the following equation:

$$(4.3) \quad E = \sqrt{(u_S)^2 + (H\{u_S\})^2}.$$

The envelope provides information about amplitudes of both the velocity signal and the Hilbert transform of the small-scale component. The results of the above procedure are presented in Fig. 6.

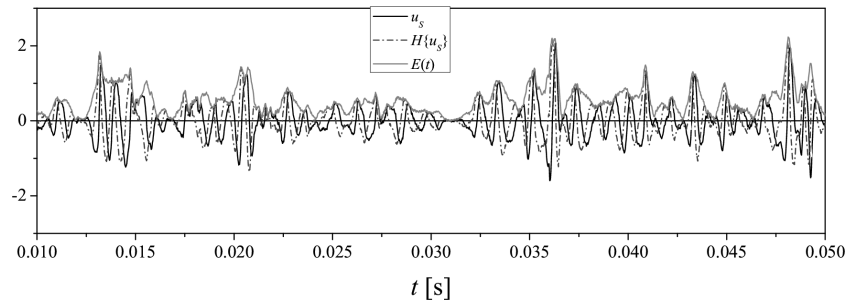


FIG. 6. Time traces of the small-scale component $u_S(t)$, its Hilbert transform $H\{u_S\}$ and envelope $E(t)$ for ZPG case and $y^+ = 5$.

In order to obtain the correlation between the envelope $E(t)$ and the large-scale component $u_L(t)$ it is necessary to use the low-pass filter for both signals. The result of this process is shown in Fig. 7. To demonstrate the relationship

between both time traces the magnitude of the envelope E_L is gained three times and shifted down by constant C which is the mean value of the envelope. As shown in Fig. 7, the time traces obtained from the signal recorded in viscous sub-layer of the ZPG flow are qualitatively highly correlated ($R = 0.535$).

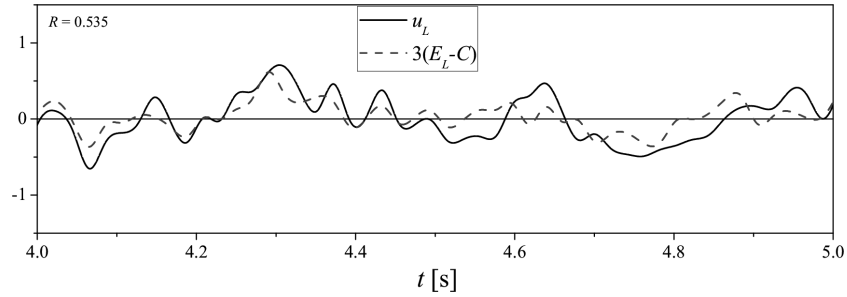


FIG. 7. Time traces of the large-scale component $u(t)_L$, and filtered envelope $E(t)_L$ for ZPG case and $y^+ = 5$.

The correlation coefficient, which is the measure of the modulation of the amplitude of the small-scale component by the large scale-component, was calculated according to equation:

$$(4.4) \quad R = \frac{\overline{E_L u_L}}{\sqrt{\overline{E_L^2}} \sqrt{\overline{u_L^2}}}.$$

The above procedure was used for all measuring locations across boundary layer thickness.

5. Result

The first step of the study was the assessment of the qualitative relationship between the small-scale and the large-scale component recorded at three relative distances from the wall, i.e., $y^+ \approx 5, 50, 800$. In order to have small- and large-scale signal components the carrier velocity signal was filtered by high- and low-pass filtering respectively. The cut-off frequency was set at timescale $\tau^+ \approx 160$ corresponding to the length scale $\lambda_x^+ \approx 1700$, which is located in the middle between the inner and outer peaks. Figure 8 presents comparison of the coupling between scales for three distances from the wall for ZPG and APG. The first location is in the sublayer ($y^+ \approx 5$), the second one in the buffer layer ($y^+ \approx 50$) and the third one in the wake layer ($y^+ \approx 800$). For each case Fig. 8 presents a carrier signal (upper time trace), large-scale signal component (middle time trace), while the lower time trace represents the small-scale signal component together with the envelope (dotted lines) corresponding to the large-scale signal.

The envelopes were shifted in the normal direction in order to easily trace the variations of magnitude of the smallscale component. For the first distance in both cases (Figs. 8a and 8b) the coupling is evident; the small-scale component signal is clearly modulated by the large-scale motions. For the ZPG case, in the buffer layer (Figs. 8c and 8d), the correlation is very low (Fig. 8c) because the amplitude of the small-scale signal is rather invariant while the envelope changes (empty spaces between small-scale signal and envelope). However, for the APG case (Fig. 8d) the small-scale to some extent varies with the envelope. This confirms assumptions about the scale's modulation in the APG TBL for low Reynolds number. For the last location (Figs. 8e and 8f), it is clearly visible that the small-scale component in both cases does not follow the shape of the envelope. As the amplitude of the large-scale component drops the magnitude of the small-scale component is enhanced and vice versa. This means that in both cases the small-scale component is inversely correlated with the large-scale component.

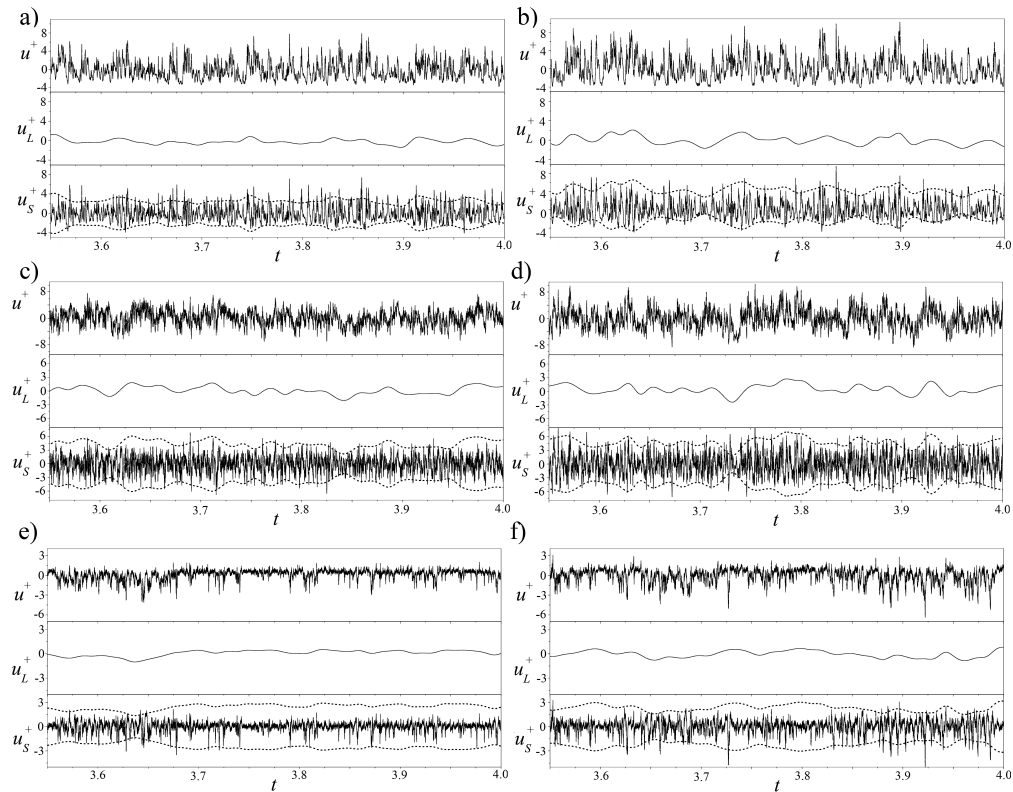


FIG. 8. Visual comparison of the coupling of the scales for three location for ZPG (a, c, e) and APG (b, d, f): (a, b) $y^+ \approx 5$, (c, d) $y^+ \approx 50$, (e, f) $y^+ \approx 800$.

The above analysis shows that even for low Reynolds number flow, but under APG conditions, there is evidence of the modulation phenomenon in the buffer layer. On the other hand, for the same Reynolds number under ZPG flow the modulation is marginal. In order to determine the strength of this modulation, the correlation coefficient R across the boundary layer thickness was calculated using Eq. (4.4).

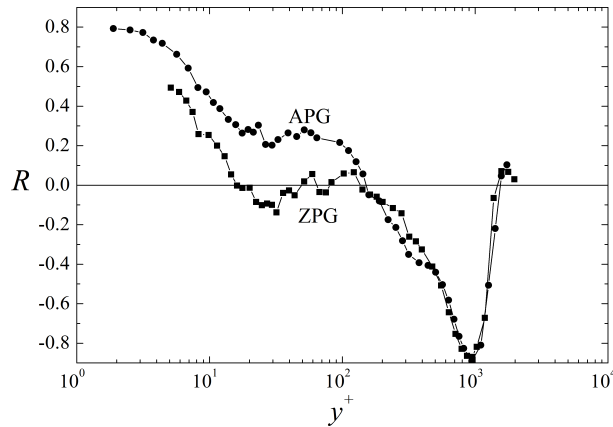


FIG. 9. Wall-normal variation of the degree R of modulation for ZPG and APG conditions at Reynolds number $Re_\tau = 1000$ (CUT).

Figure 9 shows the correlation R coefficient distributions for two analysed cross-sections from the ZPG and APG regions. For comparison the literature data taken from [1] were presented in Fig. 10. As it is seen (Figs. 9 and 10) the correlation curve R has a characteristic shape with the maximum in the viscous sub-layer, the minimum at the edge of boundary layer and a local plateau in the buffer layer. It can be noticed, however, that for APG flow the correlation between scales, for that region, is relatively high ($R \approx 0.3$), whereas for ZPG flow it has a value close to zero. The literature data (Fig. 10) exhibits also the elevation of R , in the buffer layer, with the Reynolds number increase. Additionally, the shift of the minimum, at the edge of boundary layer towards higher y^+ values, is observed. It seems that extremes of the correlation function in the viscous sub-layer and at the edge of boundary layer appear regardless of zero or adverse pressure gradients (Figs. 9 and 10). It is worth noting the intersection of R distribution with y^+ axis in the log layer coincides with the location of the outer peak of $u'u'$ distributions. According to [1] this region is probably source location of the modulation.

The reason for the strong correlation near the wall in the APG flow is twofold. On the one hand, structures already formed in packets before APG region, ex-

pand under APG conditions, and are responsible for the outer peak of $u'u'$ and the modulating effect. On the other hand, the weakening of the inner peak in the APG region (what is not observed for ZPG flows) allows the strong large-scale structures, responsible for the outer peak, to change the momentum near the wall altering the turbulence production. In summary, it is worth noting that for the ZPG case the shape of R function is similar to that observed in Fig. 10 for the lowest Reynolds number case ($Re_\tau = 2800$). In turn, for the APG case (Fig. 9, $Re_\tau = 1000$) the shape is similar to that observed for high Reynolds number flows (Fig. 10, $Re_\tau = 13\,600, 19\,000$). The similar behaviour of amplitude modulation for moderate APG was shown in [8], where the modulation effect in the buffer layer was however weaker in comparison to the presented data.

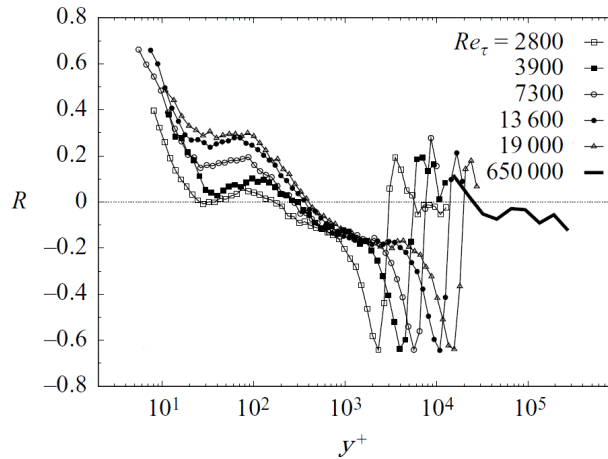


FIG. 10. Wall-normal variation of the degree R of modulation for several Reynolds numbers [1].

A strong correlation relationship between small- and large-scale structures allows us to formulate a simple model of the modulation process in the APG TBL presented in Fig. 11. Of course, due to the limited amount of data it could be treated only as a hypothesis, to be confirmed by the further study. According to this model, the large-scale structure has comparable length scale in the y direction to δ . Occurrence of such a structure has been suggested in [4]. They have proposed a conceptual scenario of packet of hairpin structures in the outer region of the TBL inducing a large-scale low speed fluid (see Fig. 1b). HUTCHINS and MARUSIC [5] clearly show that the footprint of this large-scale “superstructure” event can extend deep into the near-wall region. In accordance with the principle of mass conservation the high-speed fluid event should appear above this packet. So, the concept of large superstructure vortices, which extend across the whole

boundary layer, is thus justified (see Fig. 11). The rotation direction of this structure is shown by grey arrows. If one can imagine the movement of such a structure in the boundary layer and then, divide the area that it occupies into four parts (quadrants), it could be assumed that near the wall the production of small-scale structures is observed in area IV, where the high momentum zone exists. It is confirmed by the time courses (right-hand side plots), where in this region the magnitude of the small-scale fluctuations is consistent with the sign of the large-scale $u_L(t)$ signal, and resulting in the positive value of R function. The opposite behaviour occurs in the outer region of the TBL (area II), where the negative values of the correlation exist. The temporary velocity deficit above the large-scale structure induced by ejection behind the large-scale vortex center enhances the shear layer at the edge of the TBL. This enhanced shear layer could produce the small-scale structures at the edge of the TBL. It is confirmed by the time courses (right-hand side plots) that in the outer region the magnitude of the small-scale fluctuations are in opposite phase to the sign of the large-scale $u_L(t)$ signal.

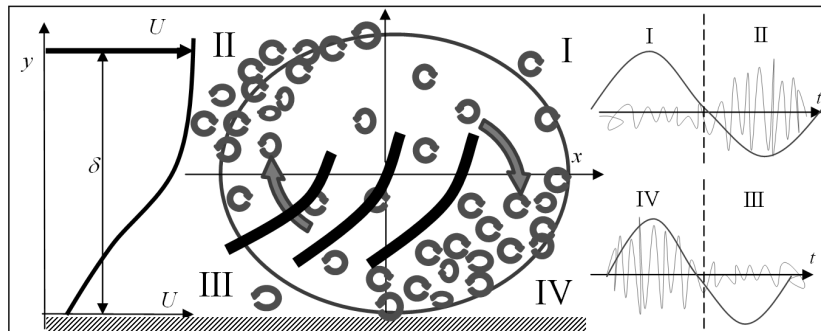


FIG. 11. Scheme of the amplitude modulation of the small-scale component by the large-scale component.

The presented model is different in its assumptions to the model proposed by MARUSIC *et al.* [14] for ZPG flow. Their model explains the coupling between small-scale structures located above and below the low and high-speed quasi-streamwise streaks located in the inner layer. Therefore, their concept is valid only near the wall, and does not explain modulation effects at the outer-edge of boundary layer. Our model clarifies, however, the mechanism of the modulation in the whole turbulent boundary layer. Enhancement of the amplitude of small-scale component occurs in areas II and IV, while the damping in areas I and III is shown on the right-hand side of the diagram (Fig. 11).

The concept of a large-scale vortex extended across the boundary layer thickness might also explain the change of movement direction of the small-scale

vortices in the APG flows. In the front of the large-scale structure, small-scale vortices are swept towards the wall while in the rear part of the structure they are ejected away from the wall. This effect was observed in [10] and [11], who studied bursting phenomenon in an APG turbulent boundary layer. They showed that under APG conditions bursting structures increase their angle of motion with respect to the wall. This conclusion was formulated based on phase averaged $\langle u \rangle$ and $\langle v \rangle$ velocity components. Additionally, the analysis of phase averaged fluctuations showed that, in comparison with ZPG, $\langle u \rangle$ velocity component is much higher than $\langle v \rangle$ velocity component, which also suggests that the angle of vortex motion is higher in the APG flows. Based on the present results as well as on data presented in [11] one can speculate that the near-wall structures are thrown from the wall to the log region by the large-scale structure and, because of that, the process is enhanced in the APG.

6. Conclusion

The influence of the adverse pressure gradient on the near-wall turbulence production cycle has been analysed. It was shown that at low Reynolds number the APG conditions has highly comparable influence on the near-wall turbulence production cycle as high Reynolds number observed for ZPG flow. It was observed that for relatively low Reynolds number ($\text{Re}_\tau \approx 1000$) and the adverse pressure gradient, apart from the inner peak of streamwise velocity fluctuations u , a second maximum located in the outer zone of turbulent boundary layer appears. It was found that the large-scale motions are much more energetic for APG compared with the ZPG case and that the pressure gradient affects mostly the outer region of the flow. Using the method proposed in [1], based on correlation function and Hilbert transform, we obtained clear evidence of a strong correlation between small inner-layer and large log-layer structures, which is similar to that observed for high-Reynolds-number, zero-pressure gradient cases. Additionally, a simple model of the modulation process occurring in APG boundary layer has been proposed. This model explains also the reason of increased angle of the bursting vortical structures motion observed in [11]. This knowledge about the modulation process could be useful for developing new methods of drag reduction in the adverse-pressure-gradient wall-bounded flows, which are often present in many engineering applications.

Acknowledgements

The research was supported by National Committee for Scientific Research Grant no. N N501 098238 (2010-2011).

References

1. R. MATHIS, N. HUTCHINS, I. MARUSIC, *Large-scale amplitude modulation of the small-scale structures in turbulent boundary layers*, J. Fluid Mech., **628**, 311, 2009.
2. T. THEODORSEN, *Mechanism of turbulence*, [in:] Proceedings of the Second Midwestern Conference on Fluid Mechanics, 1–18, 1952.
3. M. STANISLAS, L. PERRET, J.-M. FOUCAUT, *Vortical structures in the turbulent boundary layer: a possible route to a universal representation*, J. Fluid Mech., **602**, 327–382, 2008.
4. R.J. ADRIAN, C.D. MEINHART, C.D. TOMKINS, *Vortex organization in the outer region of the turbulent boundary layer*, J. Fluid Mech., **422**, 1–54, 2000.
5. N. HUTCHINS, I. MARUSIC, *Evidence of very long meandering features in the logarithmic region of turbulent boundary layers*, J. Fluid Mech., **579**, 1–28, 2007.
6. B. GANAPATHISUBRAMANI, E.K. LONGMIRE, I. MARUSIC, *Characteristics of vortex packets in turbulent boundary layers*, J. Fluid Mech., **478**, 35–46, 2003.
7. S.J. KLINE, W.C. REYNOLDS, F.A. SCHRAUB, P.W. RUNDSTADLER, *The structure of turbulent boundary layers*, J. Fluid Mech., **30**, 741–773, 1967.
8. Z. HARUN, J.P. MONTY, R. MATHIS, I. MARUSIC, *Pressure gradient effects on the large-scale structure of turbulent boundary layers*, J. Fluid Mech., **715**, 477–498, 2013.
9. M. MATERNY, A. DRÓZDŹ, S. DROBNIAK, W. ELSNER, *Experimental analysis of turbulent boundary layer under the influence of adverse pressure gradient*, Arch. Mech., **60**, 449–466, 2008.
10. A. DRÓZDŹ, W. ELSNER, S. DROBNIAK, *Application of VITA technique for detection of the organized structures present in a turbulent boundary layer under an adverse pressure gradient*, Arch. Mech., **63**, 183–199, 2011.
11. A. DRÓZDŹ, W. ELSNER, *Detection of coherent structures in a turbulent boundary layer with zero, favourable and adverse pressure gradients*, Journal of Physics: Conference Series, **318**, 062007, 2011.
12. S. GORDEYEV, *POD, LSE and Wavelet decomposition: Literature Review*, POD, LSE and Wavelet Decomposition: Literature Review, 2000.
13. J.P. MONTY, Z. HARUN, I. MARUSIC, *A parametric study of adverse pressure gradient turbulent boundary layers*, International Journal of Heat and Fluid Flow, **32**, 575–585, 2011.
14. I. MARUSIC, R. MATHIS, N. HUTCHINS *Predictive model for wall-bounded turbulent flow*, Science, **329**, 193–196, 2010.

Received November 19, 2012; final revised version August 16, 2013.
